Ferrofluid patterns in a radial magnetic field: Linear stability, nonlinear dynamics, and exact solutions

Rafael M. Oliveira and José A. Miranda*
Departamento de Física, LFTC, Universidade Federal de Pernambuco, Recife, Pernambuco 50670-901 Brazil

Eduardo S. G. Leandro
Departamento de Matemática, Universidade Federal de Pernambuco, Recife, Pernambuco 50740-540 Brazil
(Received 26 September 2007; published 14 January 2008)

The response of a ferrofluid droplet to a radial magnetic field is investigated, when the droplet is confined in a Hele-Shaw cell. We study how the stability properties of the interface and the shape of the emerging patterns react to the action of the magnetic field. At early linear stages, it is found that the radial field is destabilizing and determines the growth of fingering structures at the interface. In the weakly nonlinear regime, we have verified that the magnetic field favors the formation of peaked patterned structures that tend to become sharper and sharper as the magnitude of the magnetic effects is increased. A more detailed account of the pattern morphology is provided by the determination of nontrivial exact stationary solutions for the problem with finite surface tension. These solutions are obtained analytically and reveal the development of interesting polygon-shaped and starfishlike patterns. For sufficiently large applied fields or magnetic susceptibilities, pinch-off phenomena are detected, tending to occur near the fingertips. We have found that the morphological features obtained from the exact solutions are consistent with our linear and weakly nonlinear predictions. By contrasting the exact solutions for ferrofluids under radial field with those obtained for rotating Hele-Shaw flows with ordinary nonmagnetic fluids, we deduce that they coincide in the limit of very small susceptibilities.

DOI: 10.1103/PhysRevE.77.016304 PACS number(s): 47.15.gp, 47.54.−r, 47.65.Cb, 47.20.Ma

I. INTRODUCTION

Ferrofluids, which are colloidal suspensions of microscopic permanent magnets, respond paramagnetically to applied fields [1]. An externally applied magnetic field tends to align the nanometer-sized magnetic particles of a ferrofluid and a net magnetization **M** develops. As a result, a magnetic force arises on **M** that depends on the gradient of the local magnetic field **H**. This local field can include contributions from the applied field as well as the demagnetizing field in the polarized ferrofluid [1–3]. The existence of a gradient in **H** is a key ingredient for producing a nonzero magnetic body force in a ferrofluid: if the local magnetic field is spatially nonuniform a volume force density $\mu_0 M \nabla H$ acts on the fluid in the direction of increasing field, where μ_0 is the permeability of free space, with $M=|\mathbf{M}|$ and $H=|\mathbf{H}|$ denoting the magnitudes of the magnetization and total magnetic field, respectively. This body force is responsible for the great sensitivity and responsiveness of ferrofluids to applied magnetic fields, making this material well suited for exploring technological applications and important scientific aspects of soft condensed matter [1–6].

The effect of a magnetic field on the stability and shape of a given ferrofluid surface is a classic problem in ferrohydrodynamics [1–6]. The behavior of the ferrofluid surface is critically dependent on the direction and magnitude of **H**. One famous example of pattern formation in ferrofluids is the one related to the Rosensweig instability [7–9], in which an initially flat free surface evolves into a hexagonal array of peaks. Another popular example, known as the labyrinthine instability [10–14], arises when a ferrofluid droplet confined in a Hele-Shaw cell is subjected to a uniform perpendicular magnetic field that induces the formation of multiply bifurcated structures. In these two important examples the action of a purely uniform applied field still results in a net destabilizing magnetic body force due to the existence of a demagnetizing field. In general, the theoretical description of such demagnetizing effects under perpendicular applied magnetic fields is quite involved, and usually defies the analytical treatment of the system during nonlinear stages of the dynamics.

On the other hand, a particularly simple magnetic field setup, produced by a current-carrying wire, points along the azimuthal direction and naturally offers a radial magnetic field gradient which is not produced by complicated demagnetizing effects. In contrast to the perpendicular field case, the azimuthal field configuration produces a magnetic force directed radially inward, so that it has a *stabilizing* nature and offers plenty of room to analytical manipulation [15]. In the context of Hele-Shaw systems, the azimuthal field suppresses fingering instabilities, leading to the emergence of peculiar diamond-ring-shaped patterns [16], and to the magnetic inhibition of interfacial cusp singularities [17,18].

Regarding the creation of other nontrivial interfacial patterns in ferrofluids, it would be desirable to have at one's disposal a sufficiently simple, but *destabilizing* magnetic field configuration, for which the effect of the magnetic interactions would not rely on complicated demagnetizing effects. One suggestive possibility could be the action of a radially directed, increasing applied magnetic field. It turns out that the study of the effect of this type of radially symmetric magnetic field on the stability of a ferrofluid surface has been relatively neglected. This is perhaps due to the ap-

*jme@df.ufpe.br

parent complexity (relative to the usual perpendicular and azimuthal cases) in experimentally implementing and theoretically modeling physical systems involving legitimately radial and destabilizing magnetic fields.

Some tentative investigations along these lines are related to terrestrial laboratory studies of surface wave propagation [19] and thermomagnetic convection [20] in spherical systems, where a ferrofluid is trapped in a spherical shell and subjected to an approximately spherically symmetric, three-dimensional magnetic force field that simulates central gravity. Unfortunately, the magnetic field produced in Refs. [19,20] is not exactly simple, being of dipolar nature, so that is not entirely radial and falls off as the radial distance is increased. Some other studies [21,22], inspired by the experimental work by Heiser and Shercliff [23], theoretically investigated the steady flow of a viscous conducting fluid (not a ferrofluid) between two coaxial cylinders under a cylindrically symmetric radial magnetic field. Once again, this particular type of radially directed magnetic field requires a somewhat unusual shaping of the poles of a permanent magnet, and decreases with increasing radial distance. A more recent study [24] addresses the linear stability of radially heated circular Couette flow of ferrofluids under an effective radial gravity, simulated by a radial magnetic field produced by a vertical stack of equally spaced disk magnets.

In this work, we consider the action of a very simple and destabilizing magnetic field configuration that is perfectly feasible experimentally, and that is purely radial in the plane of the Hele-Shaw cell. This specific magnetic field configuration can be generated by a pair of identical Helmholtz coils whose currents are equal and flow in opposite directions. This is colloquially known as an "anti-Helmholtz" configuration: at the mid-distance between the coils a magnetic field is produced which is zero at the axis of symmetry of the coils, and increases linearly with the radial distance. This magnetic field configuration has been extensively used to produce magnetic traps for neutral atoms and molecules [25–27], but amazingly enough has been overlooked by the magnetic fluid community as a promising and simple tool to study the development of interesting interfacial patterns in ferrofluids.

We examine the situation in which an initially circular ferrofluid droplet is surrounded by a nonmagnetic fluid in a Hele-Shaw cell, while a radial magnetic field is applied in the plane of the cell (Fig. 1). Our main goal is to try to gain analytical insight into the fingering formation process. In Sec. II we apply a perturbative mode-coupling theory to derive coupled, nonlinear, ordinary differential equations governing the time evolution of Fourier amplitudes. The linear stability analysis of the system is presented in Sec. III, revealing the destabilizing role of the radial magnetic field, and allowing one to predict the typical number of emerging fingering structures. We also show that important information about the behavior of the arising fingers can be extracted already at weakly nonlinear stages of the dynamics: it has been verified that the action of increasingly larger magnetic effects would result in the patterned structures containing sharp fingers.

Remarkably, unlike most common situations involving pattern formation in confined ferrofluids, we have been able to identify a family of exact stationary solutions (with *nonzero* surface tension) for this problem. Section IV indicates how the vortex-sheet formalism for Hele-Shaw problems [28] can be used to access such shape solutions, which are obtained when magnetic and capillary forces are exactly matched at the interface. We have approached the problem analytically, and showed that it admits explicit integration, allowing new analytical insights about the morphology of the resulting patterns. A representative collection of possible solutions is presented, revealing the formation of suggestive polygon-shaped and starfishlike patterns. For these structures, a pinch-off phenomenon may take place near the fingertips, if large magnetic effects are involved. Finally, an alluring connection between the exact solutions induced by a radial magnetic field and those produced by nonmagnetic means through centrifugal forces is discussed. Our main conclusions and perspectives are summarized in Sec. V.

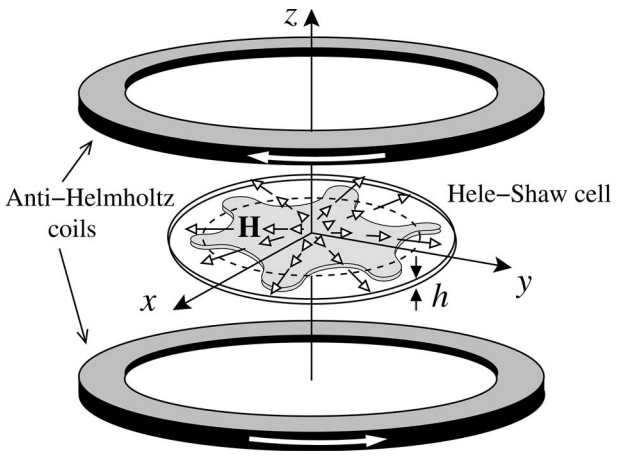

FIG. 1. Schematic illustration of the anti-Helmholtz geometry and the Hele-Shaw cell setup. The currents in the coils are equal and flow in opposite directions, producing a magnetic field **H** pointing radially outward in the plane of the Hele-Shaw cell ($z=0$ plane) as given by Eq. (1). The inner fluid is a ferrofluid (in gray), and the outer fluid is nonmagnetic. Initially, the ferrofluid droplet has a circular shape of radius R (dashed curve), but may deform due to the action of the radial magnetic field.

II. PERTURBATIVE MODE-COUPLING APPROACH

The geometry of the problem is sketched in Fig. 1: an incompressible, Newtonian ferrofluid droplet of radius R and viscosity η_2 is surrounded by a nonmagnetic fluid of viscosity η_1. The fluids flow between two narrowly spaced flat plates of a Hele-Shaw cell, located at $z=+h/2$ (upper plate) and $z=-h/2$ (lower plate). The plate spacing is represented by h, which is considered the smallest length scale in the problem. The surface tension between the fluids is nonzero and denoted by σ. We consider the action of a radial magnetic field given by

$$\mathbf{H} = H_0 r \hat{\mathbf{r}}, \tag{1}$$

where $r=\sqrt{x^2+y^2}$ is the radial distance from the origin of the coordinate system (located at the center of the droplet), H_0 is

a constant, and $\hat{\mathbf{r}}$ is a unit vector in the radial direction. As commented in Sec. I the experimental [25,27] and theoretical [26] conditions required to produce such a radial magnetic field have been discussed in a different context, where it is used to build magnetic traps for neutral atoms and molecules. The magnetic field arrangement consists of two identical coaxial Helmholtz coils whose currents are equal and flow in opposite directions (anti-Helmholtz configuration). The flat Hele-Shaw cell is coaxial with (and parallel to) the coils and placed in the $z=0$ plane midway between them (see Fig. 1).

Despite the spatial variation of applied magnetic fields [like the one expressed in Eq. (1)], the usual ferrofluids behave as Newtonian fluids [1,2], so that our study does not cover eventual non-Newtonian rheological effects due to magnetic forces. However, denser and more strongly magnetized ferrofluids were recently found to display interesting non-Newtonian behavior, including shear thinning and normal stress differences [31]. The theoretical investigation of such complex non-Newtonian properties in magnetic fluids is a challenging topic, being a subject of current debate and interest [32], but goes beyond the scope of our work.

Under such circumstances, the magnetic field is zero at the center of the ferrofluid droplet and rises linearly as prescribed by Eq. (1). This expression is valid and accurate as long as the radii of the coils are considerably larger than the typical radial distance under consideration. This assumption is consistent with existing experimental Hele-Shaw setups involving ferrofluids under uniform perpendicular applied fields (created by the usual Helmholtz coil pairs with currents flowing in the same direction), where the radius of a coil is typically 30 times larger than the radius of the ferrofluid droplet [29,30]. Of course, this type of radially increasing magnetic field could also be produced by placing the north poles of two very long permanent magnets facing each other, as experimentally implemented in Refs. [33–35].

Due to the action of the radial magnetic field (1) the fluid-fluid interface may deform, and its perturbed shape is described as $\mathcal{R}(\varphi,t)=R+\zeta(\varphi,t)$, where $\zeta(\varphi,t)=\Sigma_{n=-\infty}^{+\infty}\zeta_n(t)\exp(in\varphi)$ represents the net interface perturbation with Fourier amplitudes $\zeta_n(t)$, with discrete azimuthal wave numbers n. The polar angle in the plane of the Hele-Shaw cell is denoted by φ. We follow the standard approximations used by other investigators [1,2,10–13] and assume that the ferrofluid is magnetized such that its magnetization is collinear with the applied field. We consider only the lowest-order effect of the magnetic interactions that would result in fluid motion. Thus, in the radial field situation, we consider only the applied field in determining the magnetization. This is well justified by the fact that the radial field is parallel to the plane of the Hele-Shaw cell, so that the formation of magnetic surface charge densities that would have been responsible for inducing demagnetizing field effects is not favored [10,13]. This is also true for confined magnetic fluids under azimuthal magnetic fields [15–18] and for ferrofluids of low magnetic susceptibility [1,2].

For the effectively two-dimensional geometry of the Hele-Shaw cell, we reduce the three-dimensional flow to an equivalent two-dimensional one by averaging the Navier-Stokes equation over the direction perpendicular to the plates (defined by the z axis). Using no-slip boundary conditions and neglecting inertial terms, one derives a modified Darcy's law as [11,13]

$$\mathbf{v}_j = -\frac{h^2}{12\eta_j}\nabla\Pi_j, \tag{2}$$

where $j=1$ (2) labels the outer (inner) fluid. The generalized pressure $\Pi_j=p_j-\Psi_j$ contains both the hydrodynamic pressure p_j and a magnetic pressure represented by a scalar potential $\Psi_j=\mu_0\chi H^2/2$, where the linear relationship $M=\chi H$ has been used, with χ denoting a constant magnetic susceptibility (recall that χ is a dimensionless quantity). For the nonmagnetic fluid $\chi=0$ and $\Psi_1=0$.

From Eq. (2) and the incompressibility condition $\nabla\cdot\mathbf{v}_j=0$ it can be verified that the velocity potential ϕ_j ($\mathbf{v}_j=-\nabla\phi_j$) obeys Laplace's equation. So the problem is then specified by the augmented pressure jump boundary condition

$$p_2 - p_1 = \sigma\kappa - \frac{1}{2}\mu_0(\mathbf{M}\cdot\mathbf{n})^2, \tag{3}$$

plus the kinematic boundary condition, which states that the normal components of each fluid's velocity are continuous at the interface

$$\mathbf{n}\cdot\nabla\phi_1 = \mathbf{n}\cdot\nabla\phi_2, \tag{4}$$

with $\mathbf{n}=\nabla[r-\mathcal{R}(\varphi,t)]/|\nabla[r-\mathcal{R}(\varphi,t)]|$ denoting the unit normal vector at the interface. The first term on the right-hand side of Eq. (3) represents the usual contribution related to surface tension and interfacial curvature κ. The second term is the so-called magnetic normal traction [1,2], which considers the influence of the normal component of the magnetization at the interface. This additional term will have an important role in determining the shape of the rising interfacial patterns under a radial magnetic field.

We define Fourier expansions for the velocity potentials, and use the boundary conditions (3) and (4) to express ϕ_j in terms of ζ_n to obtain a dimensionless mode-coupling equation for the system (for $n\neq 0$) accurate to second order in the perturbation amplitudes

$$\frac{d\zeta_n}{dt} = \lambda(n)\zeta_n + \sum_{n'\neq 0}[F(n,n') + \lambda(n')G(n,n')]\zeta_{n'}\zeta_{n-n'}, \tag{5}$$

where

$$\lambda(n) = |n|\left(N_B\chi(1+\chi) - \frac{1}{R^3}(n^2-1)\right) \tag{6}$$

denotes the linear growth rate, and

$$F(n,n') = \frac{|n|}{R}\left[\frac{N_B}{2}\chi\{1+\chi[1+n'(n-n')]\} - \frac{1}{R^3}\left(1-\frac{n'}{2}(3n'+n)\right)\right], \tag{7}$$

$$G(n,n') = \frac{1}{R}\{\mathcal{A}|n|[\mathrm{sgn}(nn') - 1] - 1\} \tag{8}$$

represent second-order mode-coupling terms. The sgn function equals ±1 according to the sign of its argument. In Eqs. (5)–(8) lengths and velocities are rescaled by h and $\sigma/[12(\eta_1+\eta_2)]$, respectively. The important parameter

$$N_B = \frac{\mu_0 H_0^2 h^3}{\sigma} \tag{9}$$

represents the dimensionless magnetic Bond number, and measures the ratio of magnetic to capillary forces. The viscosity contrast is given by $\mathcal{A}=(\eta_2-\eta_1)/(\eta_2+\eta_1)$.

III. LINEAR AND WEAKLY NONLINEAR PREDICTIONS

We use Eq. (5) to examine how the development of interfacial instabilities at early stages of the pattern formation is influenced by the radial magnetic field. We begin by inspecting the linear growth rate: since a positive $\lambda(n)$ leads to an unstable interface, Eq. (6) tells us that, since N_B and χ are positive, these two factors are destabilizing. In other words, the interface can be destabilized as a consequence of the action of two different magnetic contributions: the first is due to the external radial magnetic field itself (through N_B), and the second is related to the magnetic susceptibility χ, which depends on the material properties of the ferrofluid sample. For ferrofluids the magnitude of the magnetic susceptibility can be as big as $\chi \sim 60-70$. By choosing an appropriate ferrofluid (that is, by tuning χ), one can presumably induce fingering development by using magnetic Bond numbers that are not necessarily large. The magnetic contribution to the growth rate tends to move the ferrofluid toward regions of higher magnetic fields, stimulating the growth of fingering structures. This is exactly the kind of effect we wanted: now we have a sufficiently simple applied magnetic field configuration, which is radial and destabilizing, and for which the relevant magnetic interactions do not rely on complicated demagnetizing effects.

At the linear level, a quantity of interest is the fastest-growing mode $n_{\max}$ given by setting $d\lambda(n)/dn=0$, which is related to the (integer) mode that produces the largest growth rate. This is the mode that will tend to dominate during early stages of the pattern formation process and perhaps determine the number of fingers produced at the interface. Figure 2 illustrates the combined influence of the radial magnetic field and the magnetic susceptibility on the mode of largest growth rate: it depicts $n_{\max}$ as a function of N_B, for three different values of χ. It is clear from Fig. 2 that for a given χ and droplet radius R the typical number of fingers increases with N_B, and that this growth with N_B is more significant for larger values of χ.

Linear analysis can be useful in picturing important aspects related to the stability of the interface. On its basis we have verified that the magnetic radial field configuration is indeed destabilizing, stimulating the formation of fingered structures at the interface. However, not much is extracted at linear stages about the morphology of the emerging ferrofluid patterns. We turn our attention to the weakly nonlinear, intermediate stages of pattern evolution, and use the full mode coupling Eq. (5) to investigate how the radial magnetic field influences the shape of the fingering patterns at the onset of nonlinear effects. For a detailed quantitative discussion about the regime of validity of the weakly nonlinear approximation for radial Hele-Shaw flows, see Ref. [36].

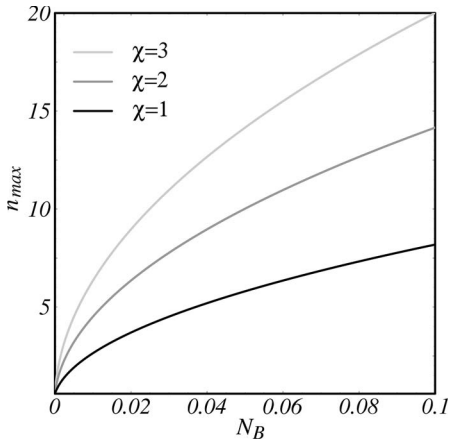

FIG. 2. $n_{\max}$ as a function of the magnetic Bond number N_B, for $R=10$ and three different values of the magnetic susceptibility: $\chi=1$ (black), 2 (dark gray), and 3 (light gray).

Inspired by an approach originally proposed in Ref. [37], which used a mode-coupling theory to analyze the development of fingertip splitting induced by injection in radial Hele-Shaw flow of nonmagnetic fluids, we focus on a mechanism controlling the finger shape behavior through magnetic means, and consider the coupling of a small number of modes. To simplify our discussion, we rewrite Eq. (5) in terms of cosine and sine modes, where the cosine $a_n=\zeta_n+\zeta_{-n}$ and sine $b_n=i(\zeta_n-\zeta_{-n})$ amplitudes are real valued. Without loss of generality we choose the phase of the fundamental mode so that $a_n>0$ and $b_n=0$. Under such circumstances, fingertip-sharpening and tip-broadening phenomena are described by considering the influence of a fundamental mode n on the growth of its harmonic $2n$ [37]. The equations of motion for the harmonic mode are written as

$$\frac{da_{2n}}{dt} = \lambda(2n)a_{2n} + \frac{1}{2}T(2n,n)a_n^2, \tag{10}$$

$$\frac{db_{2n}}{dt} = \lambda(2n)b_{2n}, \tag{11}$$

where the fingertip function is defined as

$$T(2n,n) = [F(2n,n) + \lambda(n)G(2n,n)]. \tag{12}$$

Since the growth of the sine mode b_{2n} is uninfluenced by a_n and does not present second-order couplings, we focus on the growth of the cosine mode a_{2n} as given by Eq. (10).

The interesting point is that the function $T(2n,n)$ controls the finger shape behavior. The sign of $T(2n,n)$ dictates whether fingertip sharpening or fingertip broadening is favored by the dynamics. From Eq. (10) we see that, if $T(2n,n)>0$, the result is a driving term of order a_n^2 forcing

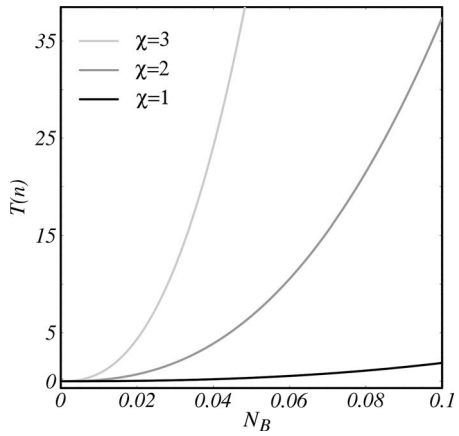

FIG. 3. Behavior of the function $T(2n,n)$ as the magnetic Bond number N_B is varied, for $R=10$ and three different values of the magnetic susceptibility: $\chi=1$ (black), 2 (dark gray), and 3 (light gray). We point out that the function $T(2n,n)$ is independent of $\mathcal{A}$.

growth of $a_{2n}>0$, the sign that is required to cause outward-pointing fingers to become sharp, favoring fingertip sharpening. In contrast, if $T(2n,n)<0$, growth of $a_{2n}<0$ is favored, leading to outward-pointing fingertip broadening. For instance, it has been shown in Ref. [37] that, for divergent radial flow of nonmagnetic fluids, one finds $T(2n,n)<0$. Thus in Ref. [37], when the harmonic is able to grow, fingertip splitting is favored, resulting in fanlike patterns similar to the ones experimentally observed in radial Hele-Shaw flows driven by injection [38].

To illustrate how the shape of the fingers responds to the action of a radial magnetic field at the onset of nonlinearity, in Fig. 3 we plot $T(2n,n)$ as a function of N_B, for three increasing values of χ, where darker colors mean lower values of χ. To ensure that both participating modes (n and $2n$) are able to grow we take $\lambda(2n)=0$. Regardless of the value of χ, we notice that $T(2n,n)\geq 0$, and that its magnitude increases as N_B assumes larger values. This weakly nonlinear result suggests that the fingers formed should become sharper and sharper as the radial magnetic field is intensified. By observing Fig. 3 it is also obvious that this effect should be stronger for larger values of χ. Notice that under the radial field the function $T(2n,n)$ is independent of the viscosity contrast $\mathcal{A}$.

Putting these linear and weakly nonlinear predictions together, one should expect the radial magnetic field to be destabilizing, and to originate interfacial patterns containing fingers with sharp tips, which increase in number and sharpness as the magnitude of the magnetic Bond number N_B or the value of the magnetic susceptibility χ is increased.

IV. EXACT SOLUTIONS OF THE PROBLEM

In this section we turn to a more specific description of the pattern morphology through the calculation of the exact solutions for this problem in ferrohydrodynamics. In addition to allowing the verification of the general predictions made in Sec. III, the exact stationary solutions reveal even more details about the shape of the patterns, including the possible occurrence of pinch-off phenomena induced by magnetic forces. Moreover, the methodology we propose to calculate these exact solutions is quite general and will certainly be useful to examine other interfacial problems in Hele-Shaw cells.

A. The vortex-sheet formalism

The Saffman-Taylor problem [39], which is related to the development of the fingering instability at the interface between two fluids of different viscosities in a Hele-Shaw cell, has been instrumental for several decades as a paradigm of interfacial pattern formation [40,41]. Undoubtedly, a contributing factor for the lasting enthusiasm toward the problem is the existence of explicit time-dependent solutions which can often be found in the zero-surface-tension limit [42–44]. Unfortunately, an analytical treatment for the problem with finite surface tension has remained very elusive, and examples of exact solutions for this case are generally scarce. A noteworthy exception is the "elasticalike" exact solutions first reported in Ref. [45], and further investigated more recently in Refs. [46,47]. This interesting family of stationary exact solutions with nonzero surface tension is obtained when capillary and viscous (or centrifugal) forces are exactly balanced at the interface.

In Refs. [46,47], this particular type of solution is found by imposing the condition of zero vorticity in the vortex-sheet formalism for Hele-Shaw flows [28]. Our goal is to apply this suggestive approach to try to find exact solutions for our radial magnetic field problem. At this point, we call the readers' attention to the fact that the study of exact solutions for pattern formation problems (with finite surface tension) in confined magnetic fluids has been largely unexplored in the literature.

The vortex-sheet representation for Hele-Shaw flows [28] explores the jump in the tangential component of the fluid velocity as one crosses the fluid-fluid interface. This approach offers an alternative and useful method to probe the morphology of the arising pattern-forming structures in the radial magnetic field problem. By writing the generalized Darcy's law [Eq. (2)] for both fluids, and then by subtracting the resulting expressions, we solve for the vortex-sheet strength $\Gamma=(\mathbf{v}_1-\mathbf{v}_2)\cdot\hat{\mathbf{s}}$ to obtain a dimensionless expression for the vorticity

$$\Gamma = 2\left[\mathcal{A}\mathbf{V}\cdot\hat{\mathbf{s}} + \partial_s\kappa - \boldsymbol{\nabla}\left(\frac{1}{2}N_B r^2\chi[1+\chi(\hat{\mathbf{n}}\cdot\hat{\mathbf{r}})^2]\right)\cdot\hat{\mathbf{s}}\right], \tag{13}$$

where $\hat{\mathbf{s}}=\partial_s\mathbf{r}$ is the unit tangent vector along the interface. In deriving Eq. (13) we have also used the pressure jump (3) and the kinematic boundary condition (4) described in Sec. II. Note that the term $(\hat{\mathbf{n}}\cdot\hat{\mathbf{r}})^2$ is reminiscent of the magnetic traction contribution in Eq. (3). Equation (13) is made dimensionless by using the same rescaling utilized to nondimensionalize Eqs. (5)–(8).

The moving boundary problem can then be written uniquely in terms of the shape of the interface. The self-consistent equation for $\mathbf{V}(s,t)$ is given by the Birkhoff integral formula [28,48]

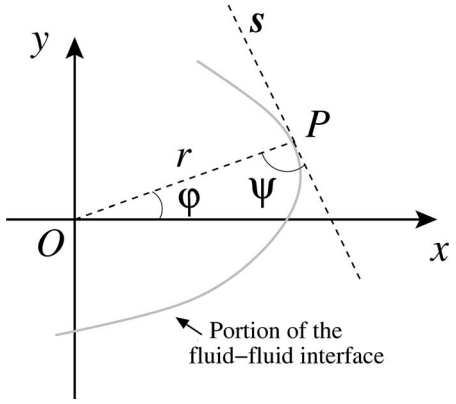

FIG. 4. Coordinate x and y axes and the angle ψ formed by the radial segment from the origin O to a generic point P at the fluid-fluid interface, and the tangent $\mathbf{s}$ to this planar curve at P. The polar angle φ and the polar radius r are also shown.

$$\mathbf{V}(s,t) = \frac{1}{2\pi}\mathrm{P}\int ds' \frac{\hat{\mathbf{z}} \times [\mathbf{r}(s,t) - \mathbf{r}(s',t)]}{|\mathbf{r}(s,t) - \mathbf{r}(s',t)|^2}\Gamma(s',t), \quad (14)$$

where P means a principal-value integral and $\hat{\mathbf{z}}$ is the unit vector along the direction perpendicular to the cell. The velocity introduced in Eq. (14) is an average velocity of the interface defined as $\mathbf{V}=(\mathbf{v}_1+\mathbf{v}_2)/2$, where $\mathbf{v}_1$ and $\mathbf{v}_2$ are the two limiting values (from both sides of the interface) of the solenoidal part of the velocity at a given point. To obtain the time evolution of the interface, Eq. (13) has to be solved with $\mathbf{V}$ given by Eq. (14), yielding a complicated integro-differential equation for the vorticity. Once Γ is known, Eq. (14) is used again to obtain $\mathbf{V}$, and then its normal component is used to update the position of the interface.

As in Refs. [46,47], instead of trying to solve the complicated integro-differential equation for the vorticity, we focus on the exact (static) solutions of Eq. (13) for finite surface tension. In a stationary state, $\mathbf{v}_1=\mathbf{v}_2=\mathbf{0}$ by definition. So, by taking $\mathbf{V}=\mathbf{0}$ in Eq. (13), and considering the condition of zero vorticity ($\Gamma=0$) we find that the curvature of the interface satisfies a nonlinear ordinary differential equation

$$\boldsymbol{\nabla}\left(\kappa - \frac{1}{2}N_B r^2 \chi[1+\chi(\hat{\mathbf{n}}\cdot\hat{\mathbf{r}})^2]\right)\cdot\hat{\mathbf{s}} = 0, \quad (15)$$

which can be integrated to obtain

$$\kappa = \kappa(r, r\sin\psi) = a + br^2 + c(r\sin\psi)^2, \quad (16)$$

where a is a constant of integration. For brevity we define $b=(N_B\chi)/2$ and $c=\chi b$. Note that b and c are both nonnegative, so in order to allow κ to change its sign along the curve, we require that $a<0$. In Eq. (16) we have used the fact that $\hat{\mathbf{n}}\cdot\hat{\mathbf{r}}=\pm\sin\psi$, where ψ is the angle between the radius vector $\hat{\mathbf{r}}$ and the tangent vector $\hat{\mathbf{s}}$ at the interface (see Fig. 4). Note that Eq. (16) does not depend on the viscosity contrast $\mathcal{A}$.

The application of the vortex-sheet formalism to our physical problem leads us to Eq. (16) which expresses the curvature of the ferrofluid interface as simply related to the radial distance r and the angle ψ. This somewhat simple expression motivated us to follow a path that is a kind of "inverse" of the one usually employed to describe the shape of planar curves. In general, a curve is given and one is asked to calculate its curvature. Here the expression for the curvature is known and written in terms of some specific parameters (r and ψ), and we want to search for the curves that satisfy such an expression.

B. Geometric approach to stationary exact solutions

We wish to study the family of planar curves whose curvature has the general form given by Eq. (16). These curves are the exact stationary solutions we are seeking which balance the competing magnetic and capillary forces at the ferrofluid interface. In order to find such solutions we begin by expressing the curvature of the interface in terms of polar coordinates r and φ (Fig. 4). By choosing r as a parameter, a differential equation for the curvature of the interface can be written as [49]

$$r\varphi'' + \varphi'(2 + r^2\varphi'^2) = \kappa(r, r\sin\psi)(1 + r^2\varphi'^2)^{3/2} \quad (17)$$

for $r>0$, where the prime indicates differentiation with respect to r. By performing a convenient change of variables $r\varphi'=\tan\psi$, and after some simplifications, we find that Eq. (17) assumes the simple form

$$(r\sin\psi)' = r\kappa(r, r\sin\psi). \quad (18)$$

Amazingly enough, if we set $w=r\sin\psi$ and use Eq. (16), we deduce at once from Eq. (18) the differential equation

$$w' = r(a + br^2 + cw^2), \quad (19)$$

which is well known as a Riccati equation [50]. It turns out that the general solution to this equation can be found through a somewhat standard procedure (which we describe in the Appendix for clarity and completeness), and can be written in closed form as a combination of the Airy functions [51] and their derivatives as

$$w(r) = -\frac{2b}{c}\left(\frac{\beta\dot{\mathrm{Ai}}(\sqrt[3]{\gamma}\rho) + \dot{\mathrm{Bi}}(\sqrt[3]{\gamma}\rho)}{\beta\mathrm{Ai}(\sqrt[3]{\gamma}\rho) + \mathrm{Bi}(\sqrt[3]{\gamma}\rho)}\right), \quad (20)$$

where $\rho=a+br^2$, $\gamma=-c/(4b^2)$, and $\beta=c_1/c_2$ is to be determined from the initial conditions r_0 and ψ_0 as the solution of the equation $w(r_0)=r_0\sin\psi_0$. In Eq. (20) Ai and Bi are Airy's functions, and the overdot notation ($\dot{\mathrm{Ai}}$ and $\dot{\mathrm{Bi}}$) denotes the derivative of these functions with respect to ρ.

By employing this geometric approach the problem of determining the shape of the interface is solved once we compute

$$\varphi(r) = \varphi_0 + \int_{r_0}^{r}\frac{1}{\tau}\tan\psi(\tau)d\tau. \quad (21)$$

This expression is quite general, in the sense that the planar curves whose curvature is given as $\kappa=\kappa(r, r\sin\psi)$ and which are parametrizable by the polar radius r are determined up to quadratures, as long as Eq. (18) is solved. The general set of curves described by Eq. (21) are opportunely expressed in terms of ψ, a parameter with a very simple geometric interpretation, being the angle between the radial

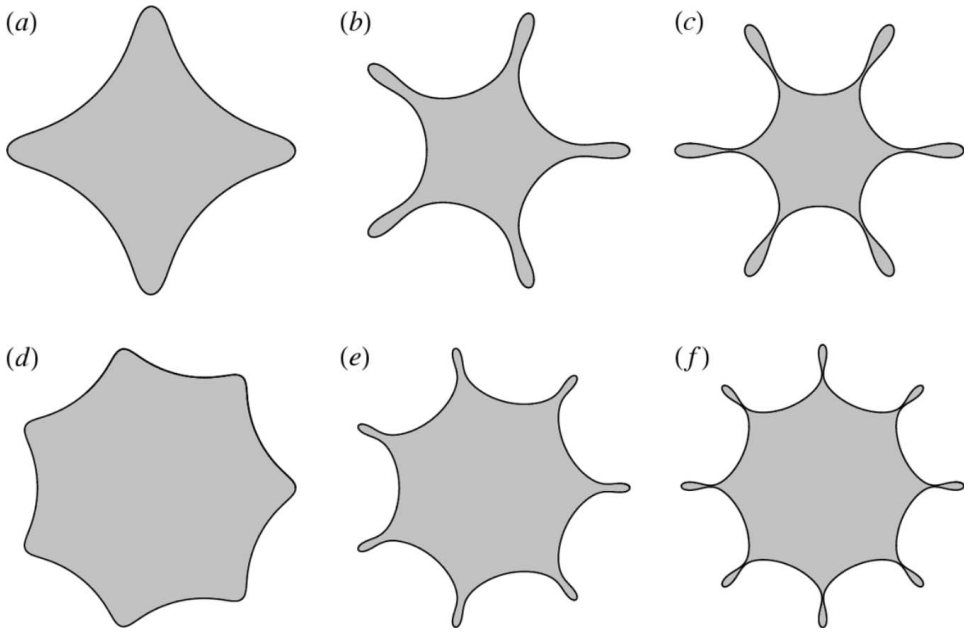

FIG. 5. Gallery of possible patterns: for $\chi=2$, $\psi_0=\pi/2$, $r_0=5.0$, $a=-1.77$, and $N_B=$ (a) 0.070, (b) 0.114, and (c) 0.119; and for $\chi=1$, $\psi_0=\pi/2$, $r_0=6.5$, $a=-6.00$, and $N_B=$ (d) 0.206, (e) 0.359, and (f) 0.367. Polygon-shaped structures [(a) and (d)], spiny starfishlike shapes [(b) and (e)], and nearly pinched interfaces [(c) and (f)] can be obtained.

and tangent directions to the curve. The radial magnetic field problem defines an important special case of this type of curve for which $\kappa(r,r\sin\psi)=a+br^2+c(r\sin\psi)^2$ [Eq. (16)]. For this specific case $\tan\psi(r)=w(r)/\sqrt{r^2-w^2(r)}$, with $w(r)$ given by Eq. (20), so that Eq. (21) is indeed a valuable theoretical tool for the study of the steady shapes. Equations (20) and (21) are central results of this work, yielding analytical access to the exact stationary solutions of the radial magnetic field problem.

C. Illustrative shape solutions

With the help of the theoretical approaches discussed in Secs. IV A and IV B, we can explore the richness behind a family of curves whose curvatures are prescribed by Eq. (16) by manipulating the relevant control parameters of the problem, namely, N_B, χ, a, r_0, and ψ_0. We show that a number of key features of the exact solutions, apparently only accessible by brute force numerical solution of the nonlinear differential Eq. (15), can be clearly revealed by properly utilizing Eq. (21). In essence the general behavior of the exact stationary shapes can be described by a "generating arc" bounded by two circles S_m and S_M whose radii are denoted as $r=r_m$ and $r=r_M$, with $0<r_m\leq r_M$. These are obtained by solving $w(r)=r$, and define the minimum (r_m) and maximum (r_M) radii of the circles delimiting an annulus in which the exact solution curve is drawn. From the existence and uniqueness theorem of solutions of ordinary differential equations [50], it follows that the solutions of Eq. (17) must possess a reflection symmetry about the rays $r=r_m$ and $r=r_M$, so the entire curve can be obtained by applying such reflections successively to the generating arc. Moreover, in order to get closed patterns, a commensurability condition needs to be satisfied [47]. When following the generating arc from r_m to r_M, the initial (φ_m) and final (φ_M) polar angles are defined, and the difference $\Delta\varphi_{mM}=\varphi_M-\varphi_m$ [obtained from Eq. (21)] must be commensurable with 2π in order for the solution to be closed. An additional condition on the variation of the polar angle between one of its critical values (which corresponds to $\psi=0$) and φ_M should be verified so that the solution is non-self-intersecting.

We begin our discussion by presenting in Fig. 5 a representative collection of possible exact stationary solutions for the problem of a confined ferrofluid droplet under the influence of a radial magnetic field. In the top row [Figs. 5(a)–5(c)] the magnetic susceptibility $\chi=2$ and N_B takes increasingly larger values (a) $N_B=0.070$, (b) $N_B=0.114$, and (c) $N_B=0.119$. The remaining parameters are $\psi_0=\pi/2$, $r_0=5.0$, and $a=-1.77$. On the other hand, in the bottom row [Figs. 5(d)–5(f)] $\chi=1$, and (d) $N_B=0.206$, (e) $N_B=0.359$, and (f) $N_B=0.367$ while $\psi_0=\pi/2$, $r_0=6.5$, and $a=-6.00$. We stress that all patterns illustrated in Fig. 5 (and also in Figs. 6 and 7) are stationary shapes, and *not* time-evolving sequences of events.

The essential features of the generated patterns can be classified as follows. For lower N_B [Figs. 5(a) and 5(d)] the exact shapes look like deformed regular polygons, whose corners are rounded and whose edges are curved inward. However, if the magnetic Bond number takes larger values [Figs. 5(b) and 5(e)] the equilibrium shapes resemble a spiny starfish, presenting sharp-tip fingers. A justification for this behavior can be given as follows. Since the applied magnetic field increases with radial distance, and because the magnetic traction term proportional to $(\hat{\mathbf{n}}\cdot\hat{\mathbf{r}})^2$ in Eq. (15) is maximized as $\hat{\mathbf{n}}$ is collinear to $\hat{\mathbf{r}}$, a larger amount of ferrofluid is added to the corners, so that the fingering structures tend to become sharper. The observation of starfishlike shapes in Figs. 5(b) and 5(e) is compatible with the weakly nonlinear prediction

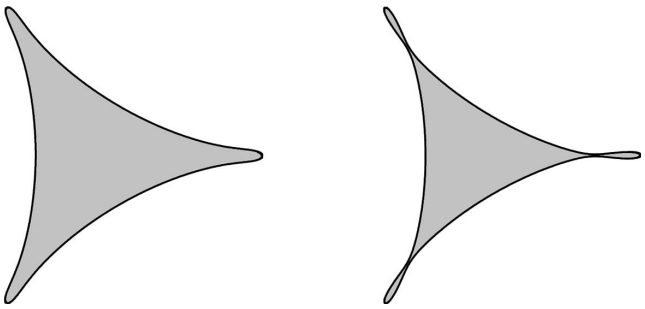

FIG. 6. Illustration of stronger tip-sharpening behavior as the magnetic susceptibility is increased: $\chi=7.00$ (left) and 8.95 (right). For both patterns the rest of the parameters and initial conditions are $N_B=0.025$, $\psi_0=\pi/2$, $r_0=5.0$,and $a=-2.00$.

made in Sec. III, which prognosticated the tendency toward fingertip sharpening.

If even higher N_B are used [Figs. 5(c) and 5(f)], the exact solutions reveal an additional interesting feature: the radially outgrowing fingers experience large magnetic effects, and the solution presents a topological singularity, eventually implying an interface pinch-off. Of course, this purely nonlinear event could not be predicted by linear and weakly nonlinear analyses. A similar pinch-off behavior has been detected in the exact solutions obtained for the rotating Hele-Shaw problem in Refs. [46,47]. It is worth noting that the phenomena of finger pinch-off and subsequent radial emission of satellite droplets have already been verified experimentally for flow of nonmagnetic fluids in rotating Hele-Shaw cells [52,53]. We point out that the linear prediction discussed in Sec. III regarding the growth of a larger number of fingers for increased N_B is consonant with the generic features of the exact solutions illustrated in Figs. 5(a)–5(c) and 5(d) and 5(e).

Another situation of interest is the response of the fingers to increased values of the magnetic susceptibility χ as all other physical parameters and initial conditions remain unchanged. In Sec. III one key prediction of the weakly nonlinear dynamics was the formation of sharper and sharper fingering structures as χ is increased. This point is reconsidered in Fig. 6: it depicts two distinct interfacial ferrofluid patterns generated by taking $\chi=7.00$ (pattern on the left) and $\chi=8.95$ (pattern on the right), for $N_B=0.025$, $\psi_0=\pi/2$, $r_0=5.0$, and $a=-2.00$. One can verify that sharper fingering structures are obtained for larger χ. Incidentally, since the magnetic traction term in Eq. (15) is proportional to χ^2, relatively small changes in χ may have significant consequences for the shape of the fingers if χ is sufficiently large.

At this point, we address a final interesting aspect of our exact solutions related to what we call the "rotating Hele-Shaw cell limit." Curiously, there is a connection between our current problem of a *magnetic* fluid droplet in a *motionless* Hele-Shaw cell and the situation involving the flow of *nonmagnetic* fluids in a *rotating* Hele-Shaw cell [46,47,52,53]. The link between these two systems comes from the realization that in both cases Darcy's law can be written in terms of a generalized pressure, like the one given by Eq. (2). The fact is that, apart from different prefactors, the scalar potentials for both problems behave like $\Psi \sim r^2$. In the rotating Hele-Shaw problem this term comes from the centrifugal contribution. On the other hand, one major difference between the two physical problems resides in the pressure boundary condition [Eq. (3)], since the magnetic traction term is present only for the case involving ferrofluids subjected to applied fields. Indeed, by contrasting the ferrofluid exact solutions illustrated in Figs. 5 and 6 with those obtained for the rotating Hele-Shaw case with nonmagnetic fluids in Refs. [46,47] (see, for instance, the right panel of Fig. 3 in Ref. [46]), one can easily verify that they are quite different. However, we should expect a greater similarity between the patterns obtained for these two different physical systems if the magnetic susceptibility is small. By inspecting Eq. (13) we conclude that the rotating Hele-Shaw cell limit can be achieved by holding fixed the product χN_B while $\chi \to 0$. In this limit our ferrohydrodynamic problem should reduce to the usual rotating Hele-Shaw situation.

This is verified explicitly in Fig. 7, where we plot a set of three ferrofluid patterns, keeping $\chi N_B=0.041$ for three small values of the magnetic susceptibility: (a) $\chi=0.028$, (b) $\chi=0.198$, and (c) $\chi=0.260$. For all these patterns $\psi_0=\pi/2$, $r_0=10.0$, and $a=-1.13$. In contrast to the patterns depicted in Figs. 5 and 6, the exact solutions illustrated in Fig. 7 have a petal-like shape, with more rounded fingers presenting bulbous ends. Notice that interface pinch-off is imminent in Fig. 7c. These low-susceptibility patterns are considerably different from the typical ones shown in Figs. 5 and 6. However, the exact solutions exhibited in Fig. 7 are very similar to the ones obtained for the actual rotating Hele-Shaw case with nonmagnetic fluids (again, see the right panel of Fig. 3 in

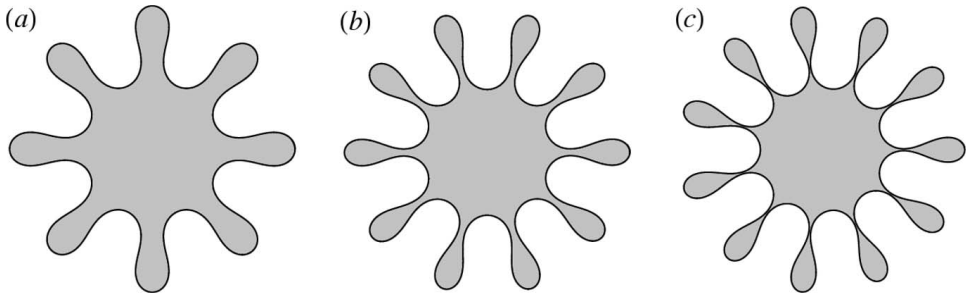

FIG. 7. Rotating Hele-Shaw cell limit. For these patterns the product $\chi N_B=0.041$, and the magnetic susceptibility is very small, χ = (a) 0.028, (b) 0.198, and (c) 0.260. For all these patterns $\psi_0=\pi/2$, $r_0=10.0$, and $a=-1.13$. These shapes are quite similar to the centrifugally induced patterns obtained in Refs. [46,47].

Ref. [46] for a comparison). In this sense, the exact magnetic fluid solutions we obtain in this work define a more general family of solutions, which includes the rotating Hele-Shaw cell as a limiting case.

We conclude this section by calling the readers' attention to the fact that, similarly to the solutions found in Refs. [45–47] for Hele-Shaw flows of nonmagnetic fluids, the exact stationary solutions for the radial magnetic field situation are unstable, and possibly very difficult to observe experimentally in a direct fashion. We refer the readers to these original studies [45–47], where the question of experimental accessibility and the practical relevance of the steady exact solutions are discussed in detail for the rectangular and rotating Hele-Shaw cell cases.

V. CONCLUSIONS

Due to the finiteness of surface tension, and also because of the usual intricate nature of the magnetic interactions in magnetic fluids, the analytic calculation of exact solutions for the problem of ferrofluid pattern formation in Hele-Shaw geometry usually becomes prohibitively complicated. However, this is not necessarily true if the applied magnetic field configuration is sufficiently simple, and if one is particularly interested in stationary shape solutions. This is precisely the situation we have studied in this work.

The radial magnetic field configuration turns out to be very simple, being generated by a pair of anti-Helmholtz coils. The ferrofluid sample is trapped in a quasi-two-dimensional Hele-Shaw cell, which is parallel and located halfway from both coils. Under such circumstances, the resulting magnetic field is legitimately radial in the Hele-Shaw cell plane. The simplicity of the situation allowed us to explore analytically a number of aspects related to the linear and weakly nonlinear regimes, as well as to derive exact steady solutions for the pattern-forming problem at hand.

Linear stability analysis reveals the destabilizing role of the radial magnetic field configuration, and predicts that the number of fingered structures should increase as the applied field, or the magnetic susceptibility of the ferrofluid sample, takes increasingly larger values. On the other hand, our weakly nonlinear results anticipate an interesting aspect of the rising fingers which should get sharper and sharper as the magnetic field (or the magnetic susceptibility) is ramped up.

In contrast to most existing problems in Hele-Shaw flow with finite surface tension, in particular those including ferrofluids, we have been able to calculate a family of exact stationary solutions for the problem. We have accomplished this task by imposing a zero-vortex-sheet strength condition at the interface, which resulted in equilibrium planar shapes whose curvatures were simply expressed in terms of the polar radius and the angle formed by the radial and tangent directions at the interface. Motivated by this fact and through a simple geometric approach, we have shown that the exact solutions for the problem satisfy an ordinary differential equation which is readily solved in closed form in terms of Airy functions, so that the shape solutions are determined up to quadratures. The result is the development of polygon-shaped and starfishlike patterns presenting fingers which become sharper as the magnetic relevant quantities of the problem are increased. These findings are consistent with the predictions of our perturbative mode-coupling theory.

For sufficiently large magnetic effects, we have verified that the sharp fingers eventually tend to break near the tips, characterizing a magnetically induced pinch-off event. We have also identified a curious connection between the radial magnetic field problem with ferrofluids and the rotating Hele-Shaw flow for nonmagnetic fluids, in the sense that the exact static solutions for both problems coincide in the limit of small magnetic susceptibilities.

A natural extension of this work would be the investigation of exact shape solutions for other magnetic field configurations, including those involving the simultaneous application of magnetic fields presenting different symmetries (radial, azimuthal, perpendicular, etc.). This would certainly result in a variety of patterns presenting still unexplored shapes and interesting dynamic behavior. Another topic of interest, associated with the imminent pinch-off detected in our exact solutions for ferrofluids, is the study of these phenomena using the framework of the lubrication theory developed to examine problems of pearling and pinching in Hele-Shaw flows with nonmagnetic fluids [54]. Finally, based on the relative simplicity of the radial magnetic field setup (anti-Helmholtz configuration) applied to Hele-Shaw geometry, as theorists we would be very interested in seeing our predictions tested with actual experiments. In summary, we hope this work will instigate further theoretical and experimental studies on this pattern formation topic in fluid dynamics.

ACKNOWLEDGMENTS

J.A.M. thanks CNPq (Brazilian Research Council) for financial support of this research through the program "Instituto do Milênio de Fluidos Complexos," Contract No. 420082/2005-0. R.M.O. acknowledges financial support from FACEPE (Fundação de Amparo à Ciência e Tecnologia do Estado de Pernambuco, Brazil) through the contract BPD No. 0007-1.05/07. J.A.M. also thanks E. Alvarez-Lacalle and D. P. Jackson for important discussions and for ongoing collaborations.

APPENDIX: SOLUTION OF RICCATI'S EQUATION

This short appendix presents the main steps leading to the solution of Riccati's differential equation (19). Let $\rho = a + br^2$ be a new parameter (notice that we must impose the condition $\rho > a$). Changing from r to ρ in Eq. (19), it follows from

$$w' = \frac{dw}{dr} = \frac{dw}{d\rho}\frac{d\rho}{dr} = 2br\dot{w}$$

that

$$2b\dot{w} = \rho + cw^2,$$

where the overdot denotes differentiation with respect to ρ. Suppose that $b \neq 0$, let $A = (1/2b)$, $B = (c/2b)$, and make the logarithmic derivative substitution

$$w = \alpha \frac{\dot{f}}{f}, \tag{A1}$$

where α is a constant to be chosen conveniently. We get, after clearing denominators,

$$\alpha(\ddot{f}f - \dot{f}^2) = A\rho f^2 + B\alpha^2 \dot{f}^2.$$

Pick $\alpha = -1/B$, so that the equation above simplifies to

$$\ddot{f} = -AB\rho f. \tag{A2}$$

This equation is known in mathematical physics [50,51] as an *Airy equation* and commonly appears in optics, quantum mechanics, and electromagnetism. If we let $\gamma = -AB = -c/4b^2$, the solutions of (A2) can be written in terms of the Airy functions as

$$f(\rho) = c_1 \mathrm{Ai}(\sqrt[3]{\gamma}\rho) + c_2 \mathrm{Bi}(\sqrt[3]{\gamma}\rho), \tag{A3}$$

where c_1 and c_2 are arbitrary constants. From (A1) and (A3) the solution of Riccati's equation (19) is obtained, as given by Eq. (20).

[1] R. E. Rosensweig, *Ferrohydrodynamics* (Cambridge University Press, Cambridge, U.K., 1985).
[2] E. Blums, A. Cebers, and M. M. Maiorov, *Magnetic Fluids* (de Gruyter, New York, 1997).
[3] B. Berkovski, *Magnetic Fluids and Applications Handbook* (Begell House, New York, 1996).
[4] J.-C. Bacri, R. Perzynski, and D. Salin, Endeavour **12**, 76 (1988).
[5] M. Seul and D. Andelman, Science **267**, 476 (1995).
[6] M. Zahn, J. Nanopart. Res. **3**, 73 (2001).
[7] M. D. Cowley and R. E. Rosensweig, J. Fluid Mech. **30**, 671 (1967).
[8] R. Friedrichs and A. Engel, Phys. Rev. E **64**, 021406 (2001).
[9] R. Richter and I. V. Barashenkov, Phys. Rev. Lett. **94**, 184503 (2005).
[10] A. O. Tsebers and M. M. Maiorov, Magnetohydrodynamics (N.Y.) **16**, 21 (1980).
[11] A. O. Cebers, Magnetohydrodynamics (N.Y.) **17**, 113 (1981).
[12] S. A. Langer, R. E. Goldstein, and D. P. Jackson, Phys. Rev. A **46**, 4894 (1992).
[13] D. P. Jackson, R. E. Goldstein, and A. O. Cebers, Phys. Rev. E **50**, 298 (1994).
[14] G. Pacitto, C. Flament, J.-C. Bacri, and M. Widom, Phys. Rev. E **62**, 7941 (2000).
[15] J. A. Miranda, Phys. Rev. E **62**, 2985 (2000).
[16] D. P. Jackson and J. A. Miranda, Phys. Rev. E **67**, 017301 (2003).
[17] J. A. Miranda and R. M. Oliveira, Phys. Rev. E **69**, 066312 (2004).
[18] R. M. Oliveira and J. A. Miranda, Phys. Rev. E **73**, 036309 (2006).
[19] D. R. Ohlsen and P. B. Rhines, J. Fluid Mech. **338**, 35 (1997).
[20] R. E. Rosensweig, J. Browaeys, J.-C. Bacri, A. Zebib, and R. Perzynski, Phys. Rev. Lett. **83**, 4904 (1999).
[21] P. Ramamoorthy, Phys. Fluids **4**, 1444 (1961).
[22] S. Y. Molokov and J. E. Allen, J. Phys. D **25**, 393 (1992); **25**, 933 (1992).
[23] W. H. Heiser and J. A. Shercliff, J. Fluid Mech. **22**, 701 (1965).
[24] R. Tagg and P. D. Weidman, Z. Angew. Math. Phys. **58**, 431 (2007).
[25] A. L. Migdall, J. V. Prodan, W. D. Phillips, T. H. Bergeman, and H. J. Metcalf, Phys. Rev. Lett. **54**, 2596 (1985).
[26] T. H. Bergeman, G. Erez, and H. J. Metcalf, Phys. Rev. A **35**, 1535 (1987).
[27] J. G. E. Harris, R. A. Michniak, S. V. Nguyen, W. C. Campbell, D. Egorov, S. E. Maxwell, L. D. van Buuren, and J. M. Doyle, Rev. Sci. Instrum. **75**, 17 (2004).
[28] G. Tryggvason and H. Aref, J. Fluid Mech. **136**, 1 (1983).
[29] D. P. Jackson, Phys. Rev. E **68**, 035301(R) (2003).
[30] N. J. Hillier and D. P. Jackson, Phys. Rev. E **75**, 036314 (2007).
[31] S. Odenbach, J. Phys.: Condens. Matter **16**, R1135 (2004).
[32] O. Müller, D. Hahn, and M. Liu, J. Phys.: Condens. Matter **18**, 1833 (2006).
[33] J. Mai, R. Kobayashi, M. Nakagawa, S. Oshima, and R. Yamane, Fluid Dyn. Res. **24**, 147 (1999).
[34] J. Mai, A. Ando, S. Oshima, R. Yamane, and H. Nishiyama, J. Phys. D **33**, 614 (2000).
[35] J. Mai, R. Yamane, W.-G. Früh, S. Oshima, and A. Ando, Eur. J. Mech. B/Fluids **21**, 237 (2002).
[36] E. Alvarez-Lacalle, E. Pauné, J. Casademunt, and J. Ortín, Phys. Rev. E **68**, 026308 (2003).
[37] J. A. Miranda and M. Widom, Physica D **120**, 315 (1998).
[38] L. Paterson, J. Fluid Mech. **113**, 513 (1981).
[39] P. G. Saffman and G. I. Taylor, Proc. R. Soc. London, Ser. A **245**, 312 (1958).
[40] D. Bensimon, L. P. Kadanoff, S. Liang, B. I. Shraiman, and C. Tang, Rev. Mod. Phys. **58**, 977 (1986); G. Homsy, Annu. Rev. Fluid Mech. **19**, 271 (1987); K. V. McCloud and J. V. Maher, Phys. Rep. **260**, 139 (1995).
[41] J. Casademunt, Chaos **14**, 809 (2004).
[42] S. K. Sarkar, Phys. Rev. A **31**, 3468 (1985).
[43] S. D. Howison, J. Fluid Mech. **167**, 439 (1986).
[44] S. P. Dawson and M. Mineev-Weinstein, Phys. Rev. E **57**, 3063 (1998).
[45] J. F. Nye, H. W. Lean, and A. N. Wright, Eur. J. Phys. **5**, 73 (1984).
[46] E. Alvarez-Lacalle, J. Ortín, and J. Casademunt, Phys. Rev. Lett. **92**, 054501 (2004).
[47] E. S. G. Leandro, R. M. Oliveira, and J. A. Miranda, Physica D (to be published).
[48] G. Birkhoff, Los Alamos Scientific Laboratory Technical Report No. LA-1862, 1954 (unpublished).
[49] H. W. Guggenheimer, *Differential Geometry* (Dover, New York, 1977).

[50] W. E. Boyce and R. C. DiPrima, *Elementary Differential Equations and Boundary Value Problems* (Wiley, New York, 1969).

[51] *Handbook of Mathematical Functions with Formulas, Graphs, and Mathematical Tables*, edited by M. Abramowitz and I. A. Stegun (Dover, New York, 1972).

[52] Ll. Carrillo, J. Soriano and J. Ortín, Phys. Fluids **12**, 1685 (2000).

[53] E. Alvarez-Lacalle, J. Ortín, and J. Casademunt, Phys. Fluids **16**, 908 (2004).

[54] R. E. Goldstein, A. I. Pesci, and M. J. Shelley, Phys. Rev. Lett. **70**, 3043 (1993).